Scaling laws for electrical contact resistance with dissimilar materials

Peng Zhang and Y. Y. Lau[a)]
Department of Nuclear Engineering and Radiological Sciences, University of Michigan, Ann Arbor, Michigan 48109-2104, USA

(Received 4 May 2010; accepted 2 June 2010; published online 26 August 2010)

This paper attempts to quantify the effects of contaminants on electrical contact resistance. Based on an idealized model, simple and explicit scaling laws for the electrical contact resistance with dissimilar materials are constructed. The model assumes arbitrary resistivity ratios and aspect ratios in the current channels and their contact region, for both Cartesian and cylindrical geometries. The scaling laws have been favorably tested in several limits, and in sample calculations using a numerical simulation code. From the scaling laws and a survey of the huge parameter space, some general conclusions are drawn on the parametric dependence of the contact resistance on the geometry and on the electrical resistivity in different regions. © *2010 American Institute of Physics*. [doi:10.1063/1.3457899]

I. INTRODUCTION

Because of the surface roughness on a microscopic scale, true contact between two pieces of conductors occurs only at the asperities (small protrusions) of two contacting surfaces. Current flows only through these asperities, which occupy a small fraction of the area of the nominal contacting surfaces. This gives rise to contact resistance,[1–4] a very important issue to thin film devices[5] and integrated circuits,[6,7] carbon nanotube based cathodes[8,9] and interconnects,[8,10] field emitters,[9,11] metal-insulator-vacuum junctions,[12] tribology,[13] wire-array z-pinches,[14] etc. On the largest scales, faulty electrical contact has caused the recent failure of the Large Hadron Collider, and similarly threatens the International Thermonuclear Experimental Reactor.[15] It is clear that contact resistance is highly random, depending on the surface roughness, on the applied pressure, on the hardness of the materials, and perhaps most importantly, on the residing oxides and contaminants at the contact.[1,2,7,14]

For decades, the fundamental model of electrical contact has been that of Holm's a-spot,[1] which consists of two semi-infinite cylinders of radius b placed together. Current can flow through them only via a "bridge" in the form of a circular disk of radius $a \ll b$. While there are statistical treatments[3] and extensions of the a-spot theory to other disk shapes,[2] Holm's zero-thickness assumption is almost always used. Most recently, an attempt has been made to relax Holm's zero-thickness assumption to include a connecting bridge of finite axial length (h) joining two metal blocks.[4] While the theory in Ref. 4 was validated in recent experiments,[16] it is restricted to the special case where the current channels and their connecting bridges are made of the *same* material, and where the current channels are of equal geometrical dimensions. Thus, the model of Ref. 4 gives no hint on the important effects of contaminants at the electrical contact.

In this paper, we substantially generalize Holm's classical a-spot theory to higher dimensions, including vastly different materials at the joints. In so doing, we also greatly extend Ref. 4 by allowing the contact region to have an arbitrary electrical resistivity, as would be expected if there were oxides or contaminants in the contact region. Figure 1 shows the geometry of such a generalized a-spot, region I, which has a finite axial length $2h$, joining two conducting current channels (II, III). This figure shows a Cartesian (cylindrical) current channel with half channel width (radius) of a, b, and c ($a \le b, a \le c$), and electrical resistivity ρ_1, ρ_2, and ρ_3. It is assumed that the axial extents of channels II and III are so long that the current flow in these channels is uniform far from the contact region, I. In this paper, we construct the scaling laws for the total electrical resistance in regions II, I, and III, including the interfaces of these regions for arbitrary values of a, b, c, h, ρ_1, ρ_2, and ρ_3 [cf. Eqs. (7) and (8)].

We shall first consider the special case $h \gg a$ for the contact region, I, so that the electrostatic fringe field at one interface (at $z=0$) has an exponentially small influence on the other interface (at $z=2h$), and vice versa. The contact resistance at the interface between regions II and I, for instance, is then the same as if regions II and I were semi-infinite in the axial (z) direction (Fig. 2). The current flow in the semi-infinite geometry shown in Fig. 2 may be formulated exactly for both Cartesian and cylindrical channels. From this exact formulation, we obtain the interface resistance between re-

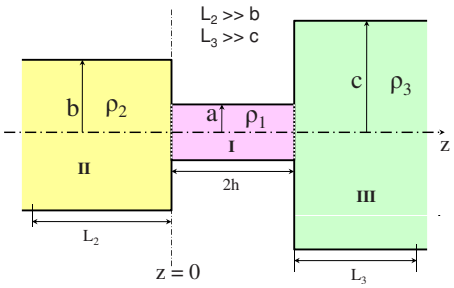

FIG. 1. (Color online) Two current channels, II and III, are made in contact through the bridge region, I, in either Cartesian or cylindrical geometries. Holm's a-spot corresponds to the cylindrical geometry with $h=0$, $a \ll b$, $a \ll c$. Current flows from left to right.

a)Electronic mail: yylau@umich.edu.

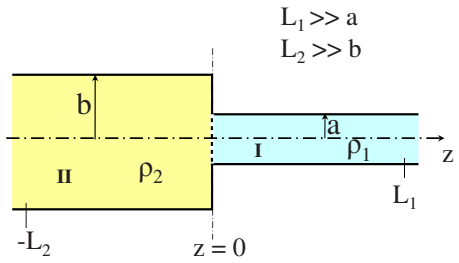

FIG. 2. (Color online) Semi-infinite current channel with dissimilar materials, regions I and II, in either Cartesian or cylindrical geometries. Current flows from left to right.

gions I and II for arbitrary values of a, b, ρ_1, and ρ_2. The vast amount of data thus collected allows us to synthesize a simple scaling law for the interface resistance. This groundwork for the interface resistance then led to our proposed scaling laws for the total electrical resistance in regions II, I, and III, for the geometry shown in Fig. 1, for general values of a, b, c, h, ρ_1, ρ_2, and ρ_3. We should remark that we have not provided an exact formulation for the general geometry shown in Fig. 1. The validity of the scaling laws for Fig. 1 is then established by our demonstration that these scaling laws are indeed an excellent approximation in several known limiting cases. They are also spot-checked against the numerical code, MAXWELL 3D.[17] From these scaling laws, we conclude that, in general, the bulk resistance in the generalized a-spot region I (Fig. 1) dominates over the resistance at the interfaces between regions I and II, and between regions I and III. The small intrinsic error in the scaling laws is also assessed.

Only the major results will be presented in the main text. Their derivations are given in the appendices. In Sec. II, the results for the contact resistance (interface resistance) between two semi-infinite current channels with dissimilar materials are presented, for both cylindrical and Cartesian geometries. The exact theory and the proposed scaling laws are found to be in excellent agreement in all regimes of the parameter space. In Sec. III, the scaling laws for the total resistance of a composite current channel (Fig. 1) are proposed and checked against several known limiting cases, and against MAXWELL 3D code. Concluding remarks are given in Sec. IV, where we indicate that the scaling laws may readily be adapted to thermal contacts under steady state condition.

II. INTERFACE RESISTANCE WITH DISSIMILAR MATERIALS

The interface resistance between regions I and II of Fig. 1, say, may be accurately evaluated when the axial extent of each region is much greater than the respective transverse dimension. It may be formulated exactly when the axial extent is semi-infinite (Fig. 2). This section presents the results of this exact formulation, together with a comparison with the proposed scaling laws, for both cylindrical and Cartesian geometry. In Fig. 2, we designate $z=0$ as the axial location of the interface, the axial length of region I is $L_1(\gg a)$ and the axial length of region II is $L_2(\gg b)$. Other parameters are defined in Fig. 2.

A. Cylindrical semi-infinite channel

For the semi-infinite cylindrical current channel (Fig. 2), we solve Laplace's equation for regions I and II, and match the boundary conditions at the interface, $z=0$. The details of the calculations are given in the Appendix A. The total resistance R from $z=-L_2$ to $z=L_1$ is found to be,

$$R = \underbrace{\frac{\rho_2 L_2}{\pi b^2}}_{\text{Bulk}} + \underbrace{\frac{\rho_2}{4a}\bar{R}_c\left(\frac{b}{a},\frac{\rho_1}{\rho_2}\right)}_{\text{Interface}} + \underbrace{\frac{\rho_1 L_1}{\pi a^2}}_{\text{Bulk}}. \tag{1}$$

In Eq. (1), the first and third term represents the bulk resistance in regions II and I, respectively. The second term represents the interface resistance between regions I and II, R_c, which is also the contact resistance for Fig. 2 (if regions I and II are regarded as two current channels). If we express this interface resistance as $R_c=(\rho_2/4a)\bar{R}_c$ for the cylindrical channel, we find that $\bar{R}_c$ depends only on the aspect ratio b/a and the resistivity ratio ρ_1/ρ_2, as explicitly displayed in Eq. (1). The *exact* expression for $\bar{R}_c$ is derived in Appendix A [cf. Eq. (A7)]. In Eq. (A7), the coefficient B_n is solved numerically in terms of ρ_1/ρ_2 and b/a, from the infinite matrix method [cf. Eq. (A4)], and, as an independent check, from the explicit iterative method for $\rho_1/\rho_2>1$ [cf. Eq. (A10)]. The two methods yield identical numerical values of B_n. These numerical values of B_n then give $\bar{R}_c$ from Eq. (A7).

The exact theory of $\bar{R}_c$ [cf. Eq. (A7)] is plotted as a function of b/a and ρ_1/ρ_2 in Fig. 3. It is clear from Fig. 3(a) that $\bar{R}_c$ increases as b/a increases, for a given ρ_1/ρ_2. It is a bit surprising, however, that for a very broad range of ρ_1/ρ_2 from 10^{-2} to 10^2, $\bar{R}_c$ varies only by a difference of $\Delta \cong 0.080\ 76$ for a given aspect ratio b/a, as is evident in Fig. 3(b). In the limit $b/a\to\infty$, this maximum variation is proven to be $\Delta=32/3\pi^2-1=0.080\ 76$ [cf. Eq. (A14)].

Based on the exact theory and its data over the huge parameter space shown in Fig. 3, we propose a simple *analytical* scaling law of $\bar{R}_c$, the normalized interface resistance, for the cylindrical semi-infinite current channel with dissimilar materials (Fig. 2),

$$\bar{R}_c\left(\frac{b}{a},\frac{\rho_1}{\rho_2}\right) \cong \bar{R}_{c0}\left(\frac{b}{a}\right)\Big|_{\text{Timsit}} + \frac{\Delta}{2}\times\left(\frac{2\rho_1}{\rho_1+\rho_2}\right) \times g\left(\frac{b}{a}\right), \quad \text{(Cylindrical)}, \tag{2}$$

$$\bar{R}_{c0}(b/a)|_{\text{Timsit}} = 1 - 1.415\ 81(a/b) + 0.063\ 22(a/b)^2 + 0.152\ 61(a/b)^3 + 0.199\ 98(a/b)^4,$$
$$g(b/a) = 1 - 0.3243(a/b)^2 - 0.6124(a/b)^4 - 1.3594(a/b)^6 + 1.2961(a/b)^8 \tag{3}$$

where $\Delta=32/3\pi^2-1=0.080\ 76$, and $\bar{R}_{c0}(x)|_{\text{Timsit}}$ is the normalized contact resistance of the a-spot derived by Timsit and Rosenfeld[2] for the following special case in Fig. 1: $h=0$, $b=c$, and $\rho_2=\rho_3$. Both $g(x)$ and $\bar{R}_{c0}(x)|_{\text{Timsit}}=0$ are

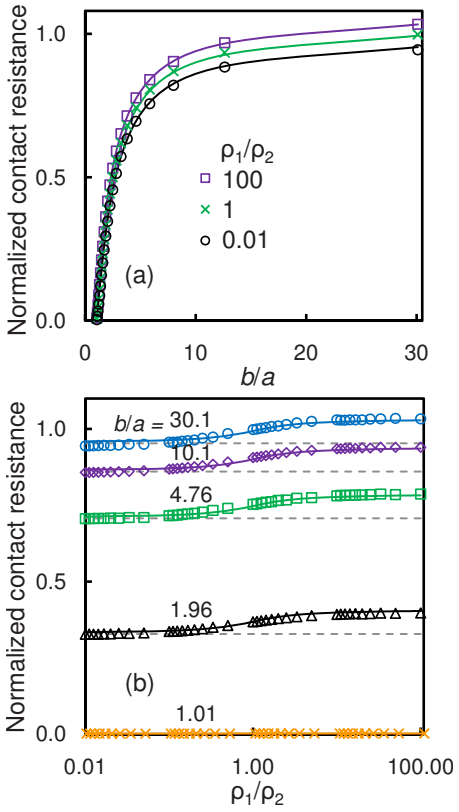

FIG. 3. (Color online) Comparison of $\bar{R}_c(b/a,\rho_1/\rho_2)$ according to the exact theory (symbols) and to the simple scaling law [Eq. (2), solid lines] for semi-infinite cylindrical current channels, I and II. (a) $\bar{R}_c$ as a function of aspect ratio b/a. (b) $\bar{R}_c$ as a function of resistivity ratio ρ_1/ρ_2. The dashed lines in (b) respresent the cylindrical a-spot theory of Timsit $[\bar{R}_{c0}(b/a)|_{\text{Timsit}}$, Eq. (3)].

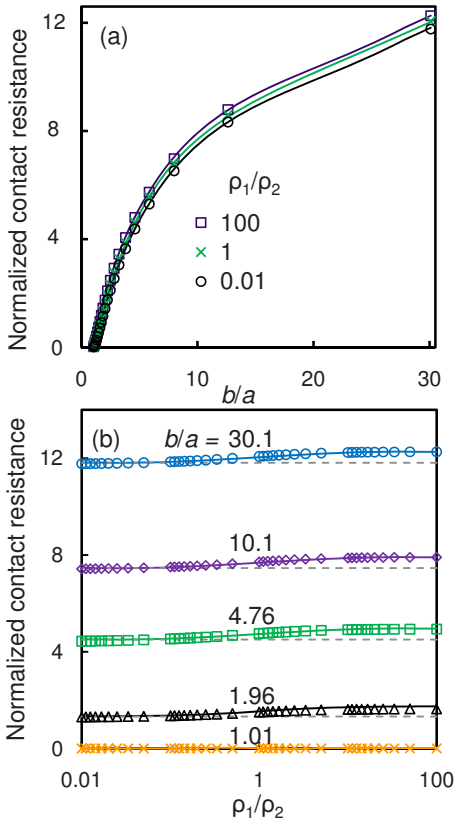

FIG. 4. (Color online) Comparison of $\bar{R}_c(b/a,\rho_1/\rho_2)$ according to the exact theory (symbols) and to the simple scaling law (Eq. (5), solid lines) for semi-infinite Cartesian current channels, I and II. (a) $\bar{R}_c$ as a function of aspect ratio b/a. (b) $\bar{R}_c$ as a function of resistivity ratio ρ_1/ρ_2. The dashed lines in (b) respresent the Cartesian a-spot theory $[\bar{R}_{c0}(b/a)|_{LTZ}$, Eq. (6)].

monotonically increasing functions of $x=b/a$ with $g(1)=0$, $g(\infty)=1$, $\bar{R}_{c0}(1)|_{\text{Timsit}}=0$, $\bar{R}_{c0}(\infty)|_{\text{Timsit}}=1$ and, therefore, Eq. (2) yields $\bar{R}_c(1,\rho_1/\rho_2)=0$, as expected of the interface resistance from Fig. 2 in the limit $b/a=1$. The scaling law of contact resistance, Eq. (2), is shown by the solid curves in Fig. 3, which compare extremely well with the exact theory, Eq. (A7), shown by the symbols, essentially for the entire range of $0<\rho_1/\rho_2<\infty$ and $b/a\geq 1$ for the cylindrical channel (Fig. 2).

B. Cartesian semi-infinite channel

Similarly, for the semi-infinite Cartesian current channel (Fig. 2), we solve Laplace's equation for regions I and II, and match the boundary conditions at the interface, $z=0$. The details of the calculations are given in the Appendix B. The total resistance R from $z=-L_2$ to $z=L_1$ is found to be,

$$R=\underbrace{\frac{\rho_2 L_2}{2b\mathrm{x}w}}_{\text{Bulk}}+\underbrace{\frac{\rho_2}{4\pi w}\bar{R}_c\left(\frac{b}{a},\frac{\rho_1}{\rho_2}\right)}_{\text{Interface}}+\underbrace{\frac{\rho_1 L_1}{2a\mathrm{x}w}}_{\text{Bulk}}. \tag{4}$$

where W denotes the channel width in the third, ignorable dimension that is perpendicular to the paper, and the rest of the symbols have been defined in Fig. 2. In Eq. (4), the first and third term represents the bulk resistance in regions II and I, respectively. The second term represents the interface resistance between regions I and II, R_c, which is also the contact resistance for Fig. 2 (if regions I and II are regarded as two current channels). If we express this interface resistance as $R_c=(\rho_2/4\pi W)\bar{R}_c$ for the Cartesian channel, we find that $\bar{R}_c$ depends only on the aspect ratio b/a and the resistivity ratio ρ_1/ρ_2 (similar to the cylindrical case) as explicitly displayed in Eq. (4). The *exact* expression for $\bar{R}_c$ is derived in Appendix B [cf. Eq. (B7)]. In Eq. (B7), the coefficient B_n is solved numerically in terms of ρ_1/ρ_2 and b/a, from the infinite matrix method [cf. Eq. (B4)], and, as an independent check, from the explicit iterative method for $\rho_1/\rho_2>1$ [cf. Eq. (B10)]. The two methods yield identical numerical values of B_n. These numerical values of B_n then give $\bar{R}_c$ from Eq. (B7).

The exact theory of $\bar{R}_c$ [cf. Eq. (B7)] is plotted as a function of b/a and ρ_1/ρ_2, as shown in Fig. 4. It is clear that from Fig. 4(a) that $\bar{R}_c$ increases as b/a increases, for a given ρ_1/ρ_2. In fact, $\bar{R}_c$ diverges logarithmically as $b/a\gg 1$, as shown in Eq. (6) and Fig. 6 below. Again, similar to the cylindrical case, it is found that for a very broad range of ρ_1/ρ_2 from 10^{-2} to 10^2, $\bar{R}_c$ varies at the most by a difference of 0.4548 for a given aspect ratio b/a of the Cartesian channel, as is evident in Fig. 4(b). The constant 0.4548 is derived in the limit $b/a\to\infty$ in Appendix B.

Based on the exact theory and its data over the huge parameter space shown in Fig. 4, we propose a simple *ana-*

lytical scaling law of $\bar{R}_c$, the normalized interface resistance, for the Cartesian semi-infinite current channel with dissimilar materials (Fig. 2),

$$\bar{R}_c\left(\frac{b}{a},\frac{\rho_1}{\rho_2}\right) \cong \bar{R}_{c0}\left(\frac{b}{a}\right)\Big|_{LTZ} + 0.2274 \times g\left(\frac{b}{a}\right) \times\left(\frac{2\rho_1}{\rho_1+\rho_2}\right), \quad \text{(Cartesian)}, \tag{5}$$

$$\bar{R}_{c0}(b/a)|_{LTZ} = 4\ln(2b/\pi a) + 4\ln(\pi/2) \times f(b/a),$$

$$f(b/a) = 0 - 0.032\,50(a/b) + 1.065\,68(a/b)^2 - 0.248\,29(a/b)^3 + 0.215\,11(a/b)^4,$$

$$g(b/a) = 1 - 2.2281(a/b)^2 + 0.1223(a/b)^4 - 0.2711(a/b)^6 + 0.3769(a/b)^8 \tag{6}$$

where $\bar{R}_{c0}(x)|_{LTZ}$ is the normalized contact resistance of the Cartesian "*a*-spot" derived by Lau, Tang, and Zhang[4] for the special case in Fig. 1: $h=0$, $b=c$, and $\rho_2=\rho_3$ [cf. last paragraph in Appendix B of the present paper]. It is the Timsit analog for the Cartesian channel [cf. Eq. (3)]. Note that in Eq. (6), $f(1)=1$, $f(\infty)=0$, $g(1)=0$, $g(\infty)=1$, $\bar{R}_{c0}(1)|_{LTZ}=0$, and $d[\bar{R}_{c0}(x)|_{LTZ}]/dx=0$ when $x=b/a=1$. Note further that, from Eq. (5), the normalized interface resistance $\bar{R}_c(1,\rho_1/\rho_2)=0$, as expected of Fig. 2 in the limit $b/a=1$. The scaling law of contact resistance, Eq. (5), is shown by the solid curves in Fig. 4, which compare extremely well with the exact theory, Eq. (B7), shown by the symbols, essentially for the entire range of $0<\rho_1/\rho_2<\infty$ and $b/a\geq 1$ for the Cartesian channel.

III. TOTAL RESISTANCE OF COMPOSITE CHANNEL

The interface resistance established for the semi-infinite channel in Sec. II prompted us to postulate a scaling law for the total resistance in a complex channel that is modeled in Fig. 1. We decompose the total resistance into bulk resistance and interface resistance. For the time being, we pretend that the scaling laws for the interface resistance given in Sec. II are also applicable when the contact region, I, has an arbitrary axial length, $2h$ (Fig. 1). We shall then verify that such an assumption introduces an error of at most 10% in the contact resistance in the worst case, $h=0$, by comparing with known results in such a limit. (Recall that the $h=0$ limit is simply the *a*-spot for the symmetric case $b=c$ and $\rho_2=\rho_3$; whereas the interface resistance was derived in Sec. II under the assumption $h\to\infty$).

Thus, in terms of the parameters defined in Fig. 1, for the cylindrical channel, we propose that the scaling law for the total electrical resistance in regions II, I, and III, including the interfaces of these regions is of the form,

$$R = \frac{\rho_2 L_2}{\pi b^2} + \frac{\rho_2}{4a}\bar{R}_c\left(\frac{b}{a},\frac{\rho_1}{\rho_2}\right) + \frac{\rho_1 \times 2h}{\pi a^2} + \frac{\rho_3}{4a}\bar{R}_c\left(\frac{c}{a},\frac{\rho_1}{\rho_3}\right) + \frac{\rho_3 L_3}{\pi c^2}, \quad \text{(Cylindrical)}, \tag{7}$$

where $\bar{R}_c$ is given by Eq. (2). Similarly, for the Cartesian channel, the proposed scaling law for the total electrical resistance in regions II, I, and III, including the interfaces of these regions reads,

$$R = \frac{\rho_2 L_2}{2b \times W} + \frac{\rho_2}{4\pi W}\bar{R}_c\left(\frac{b}{a},\frac{\rho_1}{\rho_2}\right) + \frac{\rho_1 \times 2h}{2a \times W} + \frac{\rho_3}{4\pi W}\bar{R}_c\left(\frac{c}{a},\frac{\rho_1}{\rho_3}\right) + \frac{\rho_3 L_3}{2c \times W}, \quad \text{(Cartesian)}, \tag{8}$$

where $\bar{R}_c$ is given by Eq. (5), and W denotes the channel width in the third, ignorable dimension that is perpendicular to the paper.

In both Eqs. (7) and (8), the first, third, and fifth term represent, respectively, the bulk resistance in regions II, I, and III. The second and fourth term represent the interface resistance, respectively, at the left interface between regions I and II, and at the right interface between regions I and III. If one considers region I as the electrical contact between current channel II and current channel III, then the second, third and fourth terms combine to give the contact resistance between these two current channels.

We shall now compare the scaling laws, Eqs. (7) and (8), with the results in various limits, and with sample calculations using a numerical code.

Case A: $h \gg a$

When the axial length ($2h$) of the contact region, I, much exceeds its transverse dimension, a, the electrostatic fringe field at one interface has an exponentially small influence on the other interface [cf. Eqs. (A1) and (B1) of the appendices]. Thus, the contact resistance at the left interface between regions II and I, for instance, is then the same as if regions II and I were semi-infinite in the axial direction, which has been discussed in great detail in Sec. II above. Similar comments apply to the contact resistance at the right interface between regions I and III. Equations (7) and (8) are then clearly valid as the five terms represent the five components of the total resistance (bulk and interface), all in series from left to right in Fig. 1.

Case B: $h \to 0$

In the opposite limit of Case A, the axial length $2h$ in region I is much smaller than a, with $h=0$ being the limiting case. In the latter limit, the third term in the right-hand side (RHS) of Eqs. (7) and (8) vanishes identically, and the contact resistance is then given by the sum of the second and fourth terms, which we compare with known results in several special cases. This is a stringent test because the interface resistance, represented by the second and the fourth terms, is derived under the assumption of $h \gg a$.

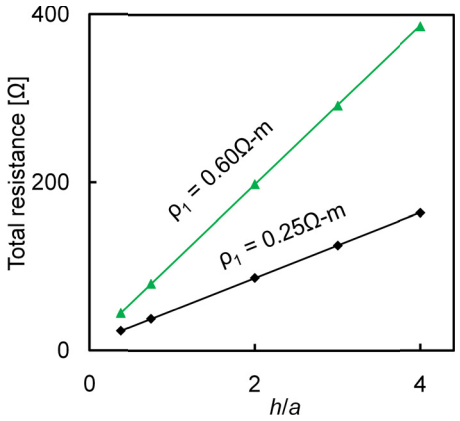

FIG. 5. (Color online) Sample calculations of the total resistance R of a cylindrical channel according to MAXWELL 3D simulation (symbols) and the scaling law, Eq. (7), (solid lines).

For the cylindrical (Cartesian) channel, the $h=0$ limit becomes the a-spot analyzed by Holm[1] and Timsit[2] (by Lau, Tang, and Zhang, cf. Fig. 6) for the symmetrical case $\rho_2=\rho_3$ and $b=c$. The scaling laws for the contact resistance, Eqs. (7) and (8), indeed become identical to these a-spot theories for $\rho_1/\rho_2 \to 0$, as shown in Eqs. (2) and (5), and also in Figs. 3(b) and 4(b). The reason is that in this symmetrical case ($\rho_2=\rho_3$, $b=c$, $h \to 0$), the current flow is perpendicular to the contact area, at the location of the a-spot, by symmetry of the geometry. Thus the entire a-spot is an equipotential surface, the same as if region I is made of perfectly conducting material ($\rho_1 \to 0$). In the opposite limit $\rho_1/\rho_2 \to \infty$, the contact resistance according to the scaling law differs from the a-spot theory by at most 7.4% (8.2%) for a cylindrical (Cartesian) channel from the data presented in Figs. 3 and 4.

In yet another limit, $h \to 0$, $b/a \to \infty$, $c/a \to \infty$, but $\rho_2 \neq \rho_3$, our scaling law, Eq. (7) for the cylindrical channel, gives a value of contact resistance that differs by at most 8% from Holm's established value of $(\rho_2+\rho_3)/4a$ for this limiting case.[1]

Case C: $\rho_1=\rho_2=\rho_3$

In this case, all channels are made of the same material. The symmetrical case $b=c$ was analyzed in great detail in Lau and Tang,[4] and was subjected to an experimental test by Gomez *et al.*[16] The scaling laws given in the present paper, aimed at vastly different values of ρ_1, ρ_2 and ρ_3, introduce a small error that is represented by the last term in Eqs. (2) and (5). This small error, already included in Figs. 3 and 4, is the price we pay for the explicit scaling law that is applicable over a huge variation in materials properties and in channel geometries, as demonstrated in these figures.

Case D: Comparison of MAXWELL 3D code

A sample comparison of the scaling law, Eq. (7), against the MAXWELL 3D (Ref. 17) simulation of a cylindrical channel is shown in Fig. 5. Excellent agreement is noted. In this example, we set $\rho_1=0.25\ \Omega$ m (and $0.60\ \Omega$ m), $\rho_2=0.038\ \Omega$ m, $\rho_3=0.001\ \Omega$ m, $a=4$ mm, $b=8$ mm, $c=10$ mm, the lengths of conductor II and III were equal, $2h$ ranging from 1.5 to 16 mm, the total axial length of the current channel simulated was fixed at 80 mm, and an excitation voltage of 10 V was applied.

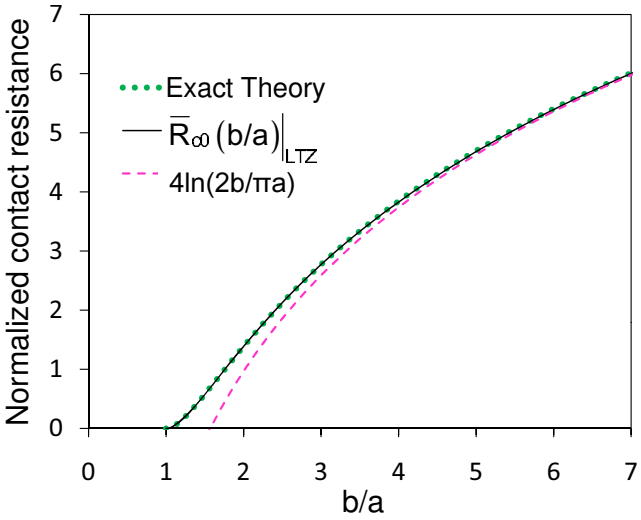

FIG. 6. (Color online) Comparison of the exact theory [Fig. 7 of Ref. 4] and the analytical formula, $\bar{R}_{c0}(x)_{LTZ}$ as given by Eq. (6) of the main text, for the normalized contact resistance of the Cartesian a-spot ($h=0$).

IV. CONCLUDING REMARKS

Having performed several checks on the validity of the scaling laws for the contact resistance joining two current channels, II and III (Fig. 1), we may now draw some general conclusions regarding the contact resistance that is comprised of the second, third and fourth terms in the RHS of the scaling laws, Eqs. (7) and (8). The third term represents the bulk resistance of the electrical contact, region I, and the second and fourth term represents the interface resistance at $z=0$ and at $z=2h$ (Fig. 1).

(a) If the electrical contact (region I) is highly resistive ($\rho_1 \gg \rho_2, \rho_1 \gg \rho_3$), then the bulk resistance [the third term on the RHS of Eqs. (7) and (8)] dominates over the interface resistance [the second and fourth term on the RHS of Eqs. (7) and (8)] once the contact region's axial length ($2h$) exceeds a few times $(\rho_2/\rho_1)a$ and $(\rho_3/\rho_1)a$.

(b) Once the geometry (a,b,c,h) is specified, the interface resistance depends mainly on the electrical resistivity of the main channel (ρ_2,ρ_3); it is insensitive to the resistivity of the contact region (ρ_1). To see this, examine the second term in Eq. (7), or in Eq. (8), for instance. This term shows that the interface resistance is linearly proportional to the current channel resistivity, ρ_2, but is quite insensitive to the ratio ρ_1/ρ_2, as shown in Fig. 3(b) or Fig. 4(b).

(c) The exact formulation for the interface resistance in Fig. 1 is quite difficult to obtain for general values of a, b, c, h, ρ_1, ρ_2, and ρ_3. The interface resistance is not easy to extract from a numerical code either, especially when there is a large contrast between ρ_1 and ρ_2 or between ρ_1 and ρ_3 or between any of the geometric dimensions h, a, b, c, L_2, and L_3. Likewise, experimen-

tal verification for the interface resistance is not easy to achieve either, if there is a large contrast in any of the above-mentioned parameters. Despite some small intrinsic errors, of order 10% or less, the simple scaling laws established in this paper then offer some new insight that is hitherto unavailable in the existing literature. They may also be used as the building block for a statistical theory.[3]

Finally, one is tempted to adapt the proposed scaling laws given in this paper to the steady state heat flow in a thermally insulated channel. This may be done with Fig. 1 by replacing the electrical conductivity $(1/\rho_j)$ with the thermal conductivity (κ_j), j = 1, 2, 3, in the different regions, assuming that the κ_j's are independent of temperature.

ACKNOWLEDGMENTS

It is a pleasure to acknowledge stimulating discussions with Matt Gomez, David French, Ronald Gilgenbach, and John Booske. This work was supported by an AFOSR grant on the Basic Physics of Distributed Plasma Discharges, AFRL, L-3 Communications Electron Device Division, and Northrop-Grumman Corporation. One of us (PZ) gratefully acknowledges a fellowship from the University of Michigan Institute for Plasma Science and Engineering.

APPENDIX A: THE CONTACT RESISTANCE OF A CONSTRICTED CYLINDRICAL CHANNEL

Referring to Fig. 2, regions I and II are semi-infinite in the axial z-direction, with the interface at $z=0$. For the cylindrical case, the Laplace's equation yields,

$$\Phi_+(r,z) = A_0 + \sum_{n=1}^{\infty} A_n J_0(\alpha_n r) e^{-\alpha_n z} - E_{+\infty} z, \quad z > 0, r \in (0,a),$$

$$\Phi_-(r,z) = \sum_{n=1}^{\infty} B_n J_0(\beta_n r) e^{+\beta_n z} - E_{-\infty} z, \quad z < 0, r \in (0,b), \quad \text{(A1)}$$

where Φ_+ and Φ_- are the electrical potential in the semi-infinite cylindrical channel I and II respectively, $E_{+\infty}$ and $E_{-\infty}$ are the uniform electric fields far from $z=0$, $J_0(x)$ is the zeroth order Bessel function of the first kind, α_n and β_n satisfy $\alpha_n a = \beta_n b = X_n$, where X_n is the nth positive zero of $J_1(x) = dJ_0(x)/dx$, and A_n and B_n are the coefficients that need to be solved. Without loss of generality, we set the coefficient B_0 to zero in Eq. (A1) for convenience. Current conservation requires that $a^2 E_{+\infty}/\rho_1 = b^2 E_{-\infty}/\rho_2$.

At the interface $z=0$, continuity of electrical potential and current density leads to the following boundary conditions:

$$\Phi_+ = \Phi_-, \quad z = 0, r \in (0,a) \quad \text{(A2a)}$$

$$\frac{1}{\rho_1}\frac{\partial \Phi_+}{\partial z} = \frac{1}{\rho_2}\frac{\partial \Phi_-}{\partial z}, \quad z = 0, \quad r \in (0,a), \quad \text{(A2b)}$$

$$\frac{\partial \Phi_-}{\partial z} = 0, \quad z = 0, \quad r \in (a,b), \quad \text{(A2c)}$$

From Eqs. (A1) and (A2a), A_n is related to B_n as,

$$A_0 = 2\sum_{n=1}^{\infty} B_n \frac{J_1(X_n a/b)}{X_n a/b}, \quad \text{(A3a)}$$

$$A_n = \sum_{m=1}^{\infty} B_m g_{mn},$$

$$g_{mn} = \frac{2}{a^2 J_0^2(X_n)} \int_0^a r J_0(\alpha_n r) J_0(\beta_m r) dr, \quad n \geq 1. \quad \text{(A3b)}$$

A change in integration variable shows that g_{mn} depends only on b/a, m, and n.

Combining Eqs. (A2b), (A2c), and (A3b), we obtain

$$B_n + \frac{a}{b}\frac{\rho_2}{\rho_1}\frac{1}{X_n J_0^2(X_n)} \sum_{m=1}^{\infty} \gamma_{mn} B_m = \frac{\rho_2}{\rho_1}\frac{2J_1(X_n a/b)}{X_n^2 J_0^2(X_n)}, \quad n = 1,2,3,\ldots, \quad \text{(A4)}$$

where

$$\gamma_{mn} = \gamma_{nm} = \sum_{l=0}^{\infty} g_{ml} g_{nl} X_l J_0^2(X_l), \quad \text{(A5)}$$

and g_{ml} and g_{nl} is in the form of the last part in Eq. (A3b). In writing Eq. (A4), we have set $aE_{+\infty} = -1$ for simplicity. It is easy to show that Eq. (A5) can be written as

$$\gamma_{nm} = \gamma_{mn} = \sum_{l=1}^{\infty} \frac{4x^2 X_m X_n X_l J_1(X_m x) J_1(X_n x)}{(X_l^2 - X_m^2 x^2)(X_l^2 - X_n^2 x^2)}, \quad x = a/b, \quad \text{(A6)}$$

which indicates that $\gamma_{nm} = \gamma_{mn} \propto 1/X_n \propto 1/n$ as $n \to \infty$. From Eq. (A4), $B_n \propto 1/X_n^2 \propto 1/n^2$ as $n \to \infty$. Therefore, the infinite matrix equation, Eq. (A4), can be inverted directly to solve for B_n with convergence guaranteed. We remark in passing that the determinant of the infinite matrix with elements γ_{mn} is zero, i.e., $\det(\gamma_{mn}) = 0$.

The total resistance between an arbitrary point $(z=L_1)$ in region I and an arbitrary point $(z=-L_2)$ in region II, both far from the interface, is $R = (\Phi_{L2} - \Phi_{L1})/I$, where $I = |\pi a^2 E_{+\infty}/\rho_1| = \pi a/\rho_1$ is the total current in the conducting channel. The contact resistance R_c, which is the difference between the total resistance R and bulk resistance $R_u = \rho_1 L_1/\pi a^2 + \rho_2 L_2/\pi b^2$, is found from Eqs. (A1) and (A3a),

$$R_c = \frac{|A_0|}{I} = \frac{\rho_2}{4a}\bar{R}_c,$$

$$\bar{R}_c = \bar{R}_c\left(\frac{b}{a}, \frac{\rho_1}{\rho_2}\right) = \frac{8}{\pi}\frac{\rho_1}{\rho_2}\left|\sum_{n=1}^{\infty} B_n \frac{J_1(X_n a/b)}{X_n a/b}\right|, \quad \text{(A7)}$$

which is the *exact* expression for the contact resistance at the interface of two semi-infinite cylindrical channels of dissimilar materials. It appears in Eq. (1) of the main text. Given the resistivity ratio ρ_1/ρ_2 and aspect ratio b/a, the coefficients B_n are solved numerically from Eq. (A4) by using either the infinite matrix method, or the explicit iterative method,

which will be discussed next. $\bar{R}_c$ is then obtained from Eq. (A7).

To solve for the coefficient B_n more efficiently, an explicit iterative method is available for $\rho_2/\rho_1<1$. From Eq. (A4), to the lowest order in ρ_2/ρ_1, we have

$$B_n^{(1)} \cong \frac{\rho_2}{\rho_1}\frac{2J_1(X_n a/b)}{X_n^2 J_0^2(X_n)}, \quad n \geq 1. \tag{A8}$$

To the next order,

$$B_n^{(2)} \cong \frac{\rho_2}{\rho_1}\frac{2J_1(X_n a/b)}{X_n^2 J_0^2(X_n)} - \frac{a}{b}\frac{\rho_2}{\rho_1}\frac{1}{X_n J_0^2(X_n)}\sum_{m=1}^{\infty}\gamma_{mn}B_m^{(1)}, \quad n \geq 1. \tag{A9}$$

To the kth order, the solution becomes,

$$B_n^{(k)} \cong \frac{\rho_2}{\rho_1}\frac{2J_1(X_n a/b)}{X_n^2 J_0^2(X_n)} - \frac{a}{b}\frac{\rho_2}{\rho_1}\frac{1}{X_n J_0^2(X_n)}\sum_{m=1}^{\infty}\gamma_{mn}B_m^{(k-1)}, \quad n \geq 1, \quad k \geq 2, \tag{A10}$$

which is the Taylor expansion of B_n in increasing power of ρ_2/ρ_1. This iterative scheme is explicit. It gives identical numerical solutions as the infinite matrix method for $\rho_2/\rho_1<1$, but converges faster. It converges very rapidly for $\rho_2/\rho_1 \ll 1$, in which case Eq. (A8) is an excellent approximation and Eq. (A7) gives,

$$\bar{R}_c\left(\frac{b}{a},\frac{\rho_1}{\rho_2}\right) \cong \frac{16}{\pi}\sum_{n=1}^{\infty}\frac{J_1^2(X_n a/b)}{X_n a/b}\frac{1}{X_n^2 J_0^2(X_n)}, \quad \rho_1/\rho_2 \gg 1. \tag{A11}$$

Equation (A11) can be further simplified if $a/b \ll 1$,

$$\bar{R}_c\left(\frac{b}{a},\frac{\rho_1}{\rho_2}\right) \cong 8\sum_{n=1}^{\infty}\frac{J_1^2(X_n a/b)}{X_n^2 a/b}, \quad \rho_1/\rho_2 \gg 1, \quad a/b \ll 1, \tag{A12}$$

since the first few terms in the infinite sum of Eq. (A11) hardly contribute, and the remaining terms may be approximated by using the asymptotic formula of $J_0(X_n)$ for large X_n. Note that to within an error of less than 0.22%,

$$X_n \cong (n+1/4)\pi, \quad n>3. \tag{A13}$$

Thus, in the limit $a/b \to 0$, we obtain from Eq. (A12),

$$\bar{R}_c\left(\frac{b}{a},\frac{\rho_1}{\rho_2}\right) \cong 8\int_1^{\infty} dn \frac{J_1^2(X_n a/b)}{X_n^2 a/b} \cong \frac{8}{\pi}\int_0^{\infty} d\xi \frac{J_1^2(\xi)}{\xi^2} = \frac{32}{3\pi^2}; \quad \rho_1/\rho_2 \gg 1, \quad a/b \to 0, \tag{A14}$$

where we have used Eq. (A13) to write the second integral, which is evaluated exactly in Whittaker and Watson.[18]

In the opposite limit, $\rho_1/\rho_2 \to 0$, $\bar{R}_c$ approaches the value of the a-spot analyzed by Holm[1] and Timsit[2] for the symmetrical case $\rho_2=\rho_3$ and $b=c$, as discussed in Sec. III, Case B, and also shown in Fig. 3(b). As $a/b \to 0$, the exact theory of symmetrical a-spot gives $\bar{R}_c=1$. Thus, the maximum range of variation in $\bar{R}_c$ for different ρ_1/ρ_2 is $\Delta=32/3\pi^2-1=0.080\,76$, as displayed in Eq. (2) of the main text, and in Fig. 3.

APPENDIX B: THE CONTACT RESISTANCE OF A CONSTRICTED CARTESIAN CHANNEL

Referring to Fig. 2, regions I and II are semi-infinite in the axial z-direction, with the interface at $z=0$. For the two-dimensional Cartesian channel, the y-axis is orthogonal to the z-axis in the plane of the paper. The Laplace's equation yields,

$$\Phi_+(y,z) = \sum_{n=0}^{\infty} A_n \cos\left(\frac{n\pi y}{a}\right)e^{-n\pi z/a} - E_{+\infty}z, \quad z>0, \quad y \in (0,a),$$

$$\Phi_-(y,z) = \sum_{n=1}^{\infty} B_n \cos\left(\frac{n\pi y}{b}\right)e^{+n\pi z/b} - E_{-\infty}z, \quad z<0, \quad y \in (0,b), \tag{B1}$$

where Φ_+ and Φ_- are the electrical potential in the semi-infinite Cartesian channel I and II respectively, $E_{+\infty}$ and $E_{-\infty}$ are the uniform electric fields far from $z=0$, and A_n and B_n are the coefficients that need to be solved. For convenience, the coefficient B_0 is set to zero in Eq. (B1). Current conservation requires that $aE_{+\infty}/\rho_1 = bE_{-\infty}/\rho_2$.

At the interface $z=0$, continuity of electrical potential and current density leads to the following boundary conditions:

$$\Phi_+ = \Phi_-, \quad z=0, \quad y \in (0,a), \tag{B2a}$$

$$\frac{1}{\rho_1}\frac{\partial \Phi_+}{\partial z} = \frac{1}{\rho_2}\frac{\partial \Phi_-}{\partial z}, \quad z=0, \quad y \in (0,a), \tag{B2b}$$

$$\frac{\partial \Phi_-}{\partial z} = 0, \quad z=0, \quad y \in (a,b), \tag{B2c}$$

From Eqs. (B1) and (B2a), A_n is related to B_n as,

$$A_0 = \sum_{n=1}^{\infty} B_n \frac{\sin(n\pi a/b)}{n\pi a/b}, \tag{B3a}$$

$$A_n = \sum_{m=1}^{\infty} B_m g_{mn},$$

$$g_{mn} = \frac{2}{a}\int_0^a \cos\left(\frac{n\pi y}{a}\right)\cos\left(\frac{m\pi y}{b}\right)dy, \quad n \geq 1. \tag{B3b}$$

A change in integration variable shows that g_{mn} depends only on b/a, m, and n.

Combining Eqs. (B2b), (B2c), and (B3b), we obtain

$$B_n + \frac{1}{n}\frac{\rho_2}{\rho_1}\sum_{m=1}^{\infty}\gamma_{nm}B_m = \frac{2}{n\pi}\frac{\rho_2}{\rho_1}\frac{\sin(n\pi a/b)}{n\pi a/b}, \quad n=1,2,3,\ldots, \tag{B4}$$

where

$$\gamma_{nm} = \gamma_{mn} = \sum_{l=0}^{\infty} l g_{nl} g_{ml}, \tag{B5}$$

and g_{ml} and g_{nl} is in the form of last part in Eq. (B3b). In writing Eq. (B4), we have set $aE_{+\infty}=-1$ for simplicity. It is easy to show that Eq. (B5) can be written as

$$\gamma_{nm} = \gamma_{mn} = \sum_{l=1}^{\infty} \frac{4mnlx^2 \sin(n\pi x)\sin(m\pi x)}{\pi^2(l^2-n^2x^2)(l^2-m^2x^2)}, \quad x = a/b, \tag{B6}$$

which indicates that $\gamma_{nm}=\gamma_{mn} \propto 1/n$ as $n \to \infty$. From Eq. (B4), $B_n \propto 1/n^2$ as $n \to \infty$. Therefore, the infinite matrix equation, (B4), can be inverted directly to solve for B_n with convergence guaranteed. We remark in passing that the determinant of the infinite matrix with elements γ_{mn} is zero, i.e., $\det(\gamma_{mn}) = 0$.

The total resistance between an arbitrary point $(z=L_1)$ in region I and an arbitrary point $(z=-L_2)$ in region II, both far from the interface, is $R=(\Phi_{L2}-\Phi_{L1})/I$, where $I=|2aW(E_{+\infty}/\rho_1)|=2W/\rho_1$ is the total current in the conducting channel, where W is the channel width in the third, ignorable dimension. The contact resistance R_c, which is the difference between the total resistance R and bulk resistance $R_u=\rho_1 L_1/2aW+\rho_2 L_2/2bW$, is found from Eqs. (B1) and (B3a),

$$R_c = \frac{|A_0|}{I} = \frac{\rho_2}{4\pi W}\bar{R}_c,$$

$$\bar{R}_c = \bar{R}_c\left(\frac{b}{a}, \frac{\rho_1}{\rho_2}\right) = 2\pi\frac{\rho_1}{\rho_2}\left|\sum_{n=1}^{\infty} B_n \frac{\sin(n\pi a/b)}{n\pi a/b}\right|, \tag{B7}$$

which is the *exact* expression for the contact resistance at the interface of two semi-infinite Cartesian channels of dissimilar materials. It appears in Eq. (4) of the main text. Given the resistivity ratio ρ_1/ρ_2 and aspect ratio b/a, the coefficients B_n are solved numerically from Eq. (B4) by using either the infinite matrix method, or the explicit iterative method, which will be discussed next. $\bar{R}_c$ is then obtained from Eq. (B7).

To solve for the coefficient B_n more efficiently, an explicit iterative method is available for $\rho_2/\rho_1 < 1$. From Eq. (B4), to the lowest order in ρ_2/ρ_1, we have

$$B_n^{(1)} \cong \frac{2}{n\pi}\frac{\rho_2}{\rho_1}\frac{\sin(n\pi a/b)}{n\pi a/b}, \quad n \geq 1. \tag{B8}$$

To the next order,

$$B_n^{(2)} \cong \frac{2}{n\pi}\frac{\rho_2}{\rho_1}\frac{\sin(n\pi a/b)}{n\pi a/b} - \frac{1}{n}\frac{\rho_2}{\rho_1}\sum_{l=1}^{\infty}\gamma_{nl}B_l^{(1)}, \quad n \geq 1. \tag{B9}$$

To the kth order, the solution becomes,

$$B_n^{(k)} \cong \frac{2}{n\pi}\frac{\rho_2}{\rho_1}\frac{\sin(n\pi a/b)}{n\pi a/b} - \frac{1}{n}\frac{\rho_2}{\rho_1}\sum_{l=1}^{\infty}\gamma_{nl}B_l^{(k-1)},$$

$$n \geq 1, \quad k \geq 2, \tag{B10}$$

which is the Taylor expansion of B_n in increasing power of ρ_2/ρ_1. This iterative scheme is explicit. It gives identical numerical solutions as the infinite matrix method for $\rho_2/\rho_1 < 1$, but converges faster. It converges very rapidly for $\rho_2/\rho_1 \ll 1$, in which case Eq. (B8) is an excellent approximation and Eq. (B7) gives,

$$\bar{R}_c\left(\frac{b}{a}, \frac{\rho_1}{\rho_2}\right) = 4\sum_{n=1}^{\infty}\frac{1}{n}\frac{\sin^2(n\pi a/b)}{(n\pi a/b)^2}, \quad \rho_1/\rho_2 \gg 1. \tag{B11}$$

In the opposite limit, $\rho_1/\rho_2 \to 0$, $\bar{R}_c$ approaches the a-spot value for the Cartesian channel that is analyzed in Ref. 4 for the symmetrical case $\rho_2=\rho_3$ and $b=c$. This is discussed in Sec. III, Case B, and also shown in Fig. 4(b). Thus, the maximum range of variation in $\bar{R}_c$ for different ρ_1/ρ_2 is the difference between Eq. (B11) and $\bar{R}_{c0}(x)|_{LTZ}$ that is given by Eq. (6) of the main text. This difference is approximately the constant 0.4548 for $b/a \gg 1$, as shown in Eq. (5) of the main text, and in Fig. 4.

Finally, we remark that the exact theory of Lau and Tang[4] for the a-spot of the Cartesian channel is recently synthesized into a useful and accurate formula, $\bar{R}_{c0}(x)|_{LTZ}$ that is given in Eq. (6) of the main text. Figure 6 shows that this new formula is virtually identical to the exact theory of Ref. 4. In Fig. 6, we also compare $\bar{R}_{c0}(x)|_{LTZ}$ with the less accurate formula derived in Ref. 4,

$$\bar{R}_c \cong 4\ln\left(\frac{2}{\pi}\frac{b}{a}\right), \quad \rho_1/\rho_2 \to 0, \quad a/b \ll 1. \tag{B12}$$

[1] R. Holm, *Electric Contact*, 4th ed. (Springer-Verlag, Berlin, 1967).
[2] R. S. Timsit, IEEE Trans. Compon. Packag. Technol. **22**, 85 (1999); A. M. Rosenfeld and R. S. Timsit, Q. Appl. Math. **39**, 405 (1981).
[3] Y. H. Jang and J. R. Barber, J. Appl. Phys. **94**, 7215 (2003).
[4] Y. Y. Lau and W. Tang, J. Appl. Phys. **105**, 124902 (2009).
[5] P. M. Hall, Thin Solid Films **1**, 277 (1968); H. Klauk, G. Schmid, W. Radlik, W. Weber, L. Zhou, C. D. Sheraw, J. A. Nichols, and T. N. Jackson, Solid-State Electron. **47**, 297 (2003).
[6] G. H. Gelinck, T. C. T. Geuns, and D. M. de Leeuw, Appl. Phys. Lett. **77**, 1487 (2000); W. J. Greig, *Integrated Circuit Packaging, Assembly and Interconnections* (Springer, New York, 2007).
[7] J.-L. Carbonero, G. Morin, and B. Cabon, IEEE Trans. Microwave Theory Tech. **43**, 2786 (1995).
[8] R. H. Baughman, A. A. Zakhidov, and W. A. de Heer, Science **297**, 787 (2002).
[9] D. Shiffler, T. K. Statum, T. W. Hussey, O. Zhou, and P. Mardahl, in *Modern Microwave and Millimeter Wave Power Electronics*, edited by R. J. Barker, J. H. Booske, N. C. Luhmann, and G. S. Nusinovich (IEEE, Piscataway, NJ, 2005), Chap. 13, p. 691; V. Vlahos, J. H. Booske, and D. Morgan, Appl. Phys. Lett. **91**, 144102 (2007).
[10] W. Wu, S. Krishnan, T. Yamada, X. Sun, P. Wilhite, R. Wu, K. Li, and C. Y. Yang, Appl. Phys. Lett. **94**, 163113 (2009); Z. Yao, C. L. Kane, and C. Dekker, Phys. Rev. Lett. **84**, 2941 (2000); D. Mann, A. Javey, J. Kong, Q. Wang, and H. Dai, Nano Lett. **3**, 1541 (2003).
[11] R. Miller, Y. Y. Lau, and J. H. Booske, Appl. Phys. Lett. **91**, 074105 (2007).
[12] V. Latham, *High Voltage Vacuum Insulation* (Academic, London, UK, 1995); N. Jordan, R. M. Gilgenbach, B. W. Hoff, and Y. Y. Lau, Rev. Sci. Instrum. **79**, 064705 (2008).
[13] P. G. Slade, *Electrical Contacts: Principles and Applications* (Dekker, New York, 1999).
[14] D. A. Chalenski, B. R. Kusse, and J. B. Greenly, Phys. Plasmas **16**, 082707 (2009); M. R. Gomez, J. C. Zier, R. M. Gilgenbach, D. M. French, W. Tang, and Y. Y. Lau, Rev. Sci. Instrum. **79**, 093512 (2008).

[15]P. Bruzzone, B. Stepanov, R. Dettwiler, and F. Staehli, IEEE Trans. Appl. Supercond. **17**, 1378 (2007); A. Nijhuis, Y. Ilyin, W. Abbas, B. ten Haken, and H. H. J. ten Kate, Cryogenics **44**, 319 (2004).
[16]M. R. Gomez, D. M. French, W. Tang, P. Zhang, Y. Y. Lau, and R. M. Gilgenbach, Appl. Phys. Lett. **95**, 072103 (2009).
[17]http://www.ansoft.com
[18]E. T. Whittaker and G. N. Watson, *A Course of Modern Analysis*, 4th ed. (Cambridge University Press, Cambridge, UK, 1927), pp. 282 and 385.